Iraqi Journal of Physics, 2025 *Vol.23, No.1, PP. 68-77*
https://doi.org/10.30723/ijp.v23i1.1334 *P-ISSN: 2070-4003*
E-ISSN: 2664-5548

Synthesis, Structural, and Optical Characterization of ZnO/SnO_2 Nanocomposites Thin Films Prepared by Spin Coating and Pulse Laser Deposition

Amna A. Al-Bayati[1a*] and Hanaa F. Al-Taay[1b]
[1]*Physics Department, College of Science for Women, University of Baghdad, Baghdad, Iraq*
Corresponding author: hanaa_flayeh@yahoo.com

Abstract
Zinc oxide/ Tin oxide (ZnO/SnO_2) nanocomposite thin films are prepared on glass substrates by spin coating and pulsed laser deposition (PLD) techniques, utilizing various ZnO/SnO_2 ratios. The fabricated thin films are exposed to annealing at 300°C to improve their crystallinity. The surface morphology, crystalline structure, and optical properties of the produced ZnO/SnO_2 nanocomposite thin films are examined. The field emission scanning emission microscopy (FESEM) images of ZnO and ZnO/SnO_2 nanocomposite thin films fabricated via the spin coating process demonstrated an increase in particle size from 11 to 18 nm when the ZnO ratio increased from 50% to 90%. The minimum particle size for samples generated via PLD was 6.5 nm, achieved with a $ZnO:SnO_2$ ratio of 70:30. The XRD results indicated that the ZnO and ZnO/SnO_2 nanocomposite thin films, prepared via spin coating and PLD methods, exhibited the hexagonal wurtzite structure of ZnO and the tetragonal structure of SnO_2. The optical energy gap of pure ZnO produced by both methods was 3.2 eV, which increased to 3.8 eV for $_{50}ZnO/_{50}SnO_2$ nanocomposite thin films prepared using the spin coating method. The energy gap of $_{70}ZnO/_{30}SnO_2$ nanocomposite thin films was 3.7 eV when employing the PLD method.

Article Info.

Keywords:
ZnO, SnO_2, Nanocomposite, PLD, Spin Coating.

Article history:
Received: Jul.07, 2024
Revised: Oct.27, 2024
Accepted: Nov.11,2024
Published:Mar.01,2025

1. Introduction
Nanocomposites are composite materials with at least one phase and dimensions in the nanoscale range. Nanocomposites are important because of their remarkable properties, which result from the synergy between component characteristics and interfacial qualities. These features appear significantly different from those of conventional micrometer-sized composites. This mainly results from the nanometer-scale component, which considerably increases the available contact surface area [1, 2].

Semiconductor oxides are essential functional materials, exhibiting adjustable characteristics and numerous technological applications. Zinc Oxide (ZnO) and Tin Oxide (SnO_2) are the two most commonly studied n-type semiconductor materials. They have high band gaps of 3.36 and 3.64 eV, which means that visible light can pass through them [3]. ZnO and SnO_2 nanocomposite materials demonstrate potential for diverse applications, including solar cells [4], optical sensors [5], light-emitting diodes [6], and photocatalysts [7]. Gas sensor devices utilize ZnO and SnO_2 due to their excellent electrical conductivity and ability to detect gases such as H_2, CO, alcohol, toluene, and methanol [8].

Various physical and chemical techniques, such as thermal evaporation, magnetron sputtering, pulsed laser deposition, spin coating, and chemical vapor deposition, can synthesize ZnO/SnO_2 nanocomposite thin films [9-13].

ZnO and SnO_2 are the most common semiconductor oxides. They have well-known physical properties, such as being stable at high temperatures, safe for the environment, chemically stable, cheap, and easy to make into nanostructured forms, which makes them useful in many areas. They still hold the interest of many researchers

today. Therefore, the purpose of this work is to create ZnO and ZnO/SnO_2 nanocomposite thin films with different amounts of SnO_2 using spin coating and pulsed laser deposition (PLD) techniques. Examine the impact of preparation strategies on the morphological, structural, and optical characteristics of ZnO/SnO_2 nanocomposites thin films.

2. Experimental Work

Glass substrate was cleaned successively using an ultrasonic bath using 2-praponal, acetone, and deionized water for 20 min each time and then dried. ZnO/SnO_2 nanocomposites prepared by spin coating and PLD using ZnO and Tin oxide SnO_2 powders with 99.9% purity. Various concentrations of composites ($_{50}ZnO/_{50}SnO_2$, $_{70}ZnO/_{30}SnO_2$, and $_{90}ZnO/_{10}SnO_2$) were dissolved in pure ethanol. The solution placed on a heating plate was stirred for 3 hours to obtain a stabilized solution. The solution was kept for 24 hours to produce a stable solution. After that, the sol-gel solution was dropped over cleaned substrates, which were then spun at 3000 rpm for 30 seconds before being heated for 10 minutes on a hot plate at 100 °C. Next, the samples were annealed for 1 hour at 300 °C before measuring their properties. Using a hydraulic press of 6.5 tons, the PLD prepared ZnO and SnO_2 powders were compressed to be the target with a diameter of 2.5 cm and a thickness of 0.4 cm. The deposition was carried out using an Nd:YAG laser with a wavelength of 1064 nm, laser energy of 800 mJ, a repetition rate of 6 Hz, and 600 pulses. The distance between the target and the substrate was 10 cm under a vacuum of 3×10^{-3} m Torr. The surface morphology of the synthesized ZnO and nanocomposite thin films was analyzed using field emission scanning electron microscopy (FESEM) (Leo-Supra 50VP, Carl Zeiss, Germany). The crystalline structure was discovered using X-ray diffraction analysis (XRD) (SHIMADZU Japan) utilizing Cu-Kα (α = 0.154 nm) radiation at a voltage of 40 kV and a current of 30 mA. The X-ray scan is conducted with 2θ ranging from 20° to 100°. The voltage is 40 kV, and the current is 30 mA. Furthermore, the optical properties were examined using an Ultraviolet-Visible Spectrophotometer (Model English Industry, UV-2601), covering a wavelength range of 200 to 1100 nm.

3. Results and Discussion

3.1. Surface Morphology

The surface morphology of pure ZnO and ZnO/SnO_2 nanocomposite thin films, with various concentrations, obtained from the spin coating and PLD methods, was analyzed using FESEM images, as illustrated in Figs. 1 and 2.

The images of nanocrystalline thin films created via spin coating clearly exhibited homogeneity, were free of cracks, and demonstrated full coverage of the substrate surface, as well as a high dispersion density of small particles on the substrate (Figs. 1 A, B, C, and D).

The PLD method for synthesizing nanocomposite thin films demonstrates that the images illustrate the non-uniform aggregation of nanoparticles during growth. Especially, Fig. 2A. In addition, Figs.2 (C and D) demonstrate that the substantial expansion of nanoparticles characterized by high density and tiny particle size.

Figs. 3 and 4 show the diameter distribution of thin films made of pure ZnO and ZnO/SnO_2 nanocomposite at different concentrations. These films were made using spin coating and PLD techniques, and the Image J program was used to figure them out. Pure ZnO exhibits a diameter range of 4 to 45 nm, with an average diameter of 12 nm. Furthermore, samples $_{50}ZnO/_{50}SnO_2$, $_{70}ZnO/_{30}SnO_2$, and $_{90}ZnO/_{10}SnO_2$ exhibited average diameters of 11, 15, and 18 nm, respectively, indicating that $_{50}ZnO/_{50}SnO_2$ possesses the smallest particle size.

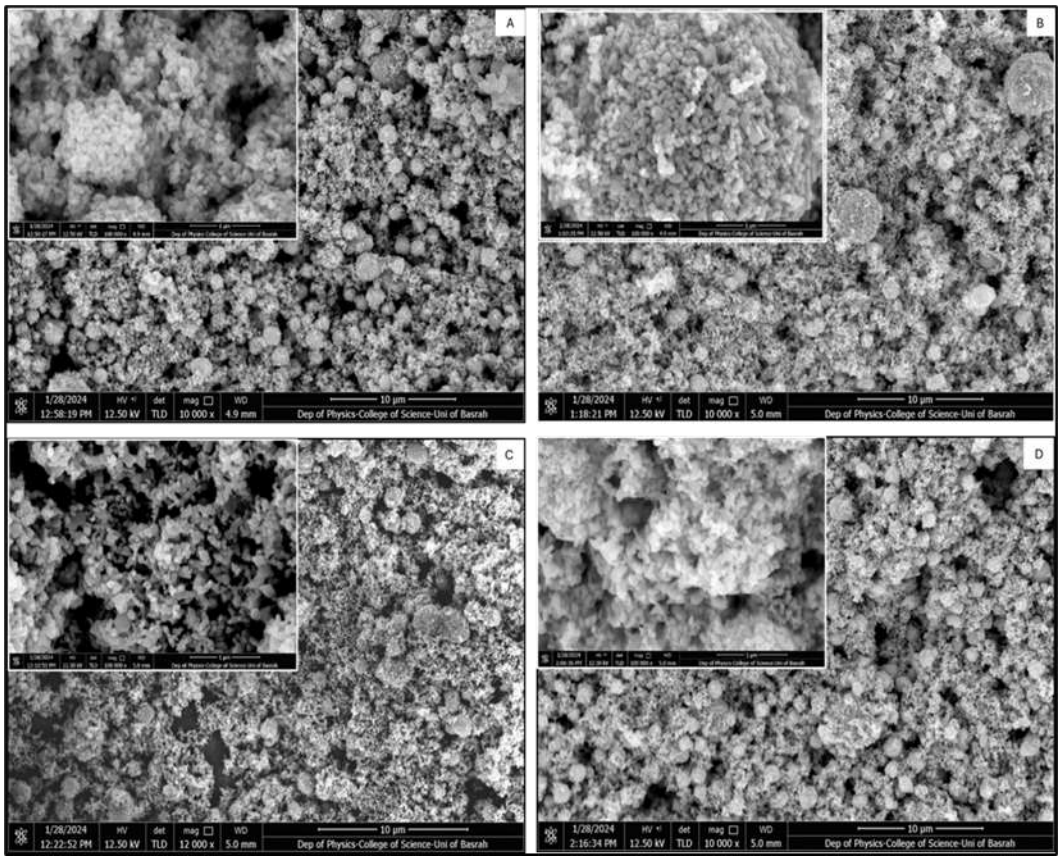

Figure 1: FESEM images show the different scale of (A) pure ZnO (B) $_{50}ZnO/_{50}SnO_2$ (C) $_{70}ZnO/_{30}SnO_2$ and (D) $_{90}ZnO/_{10}SnO_2$ prepared by spin coating.

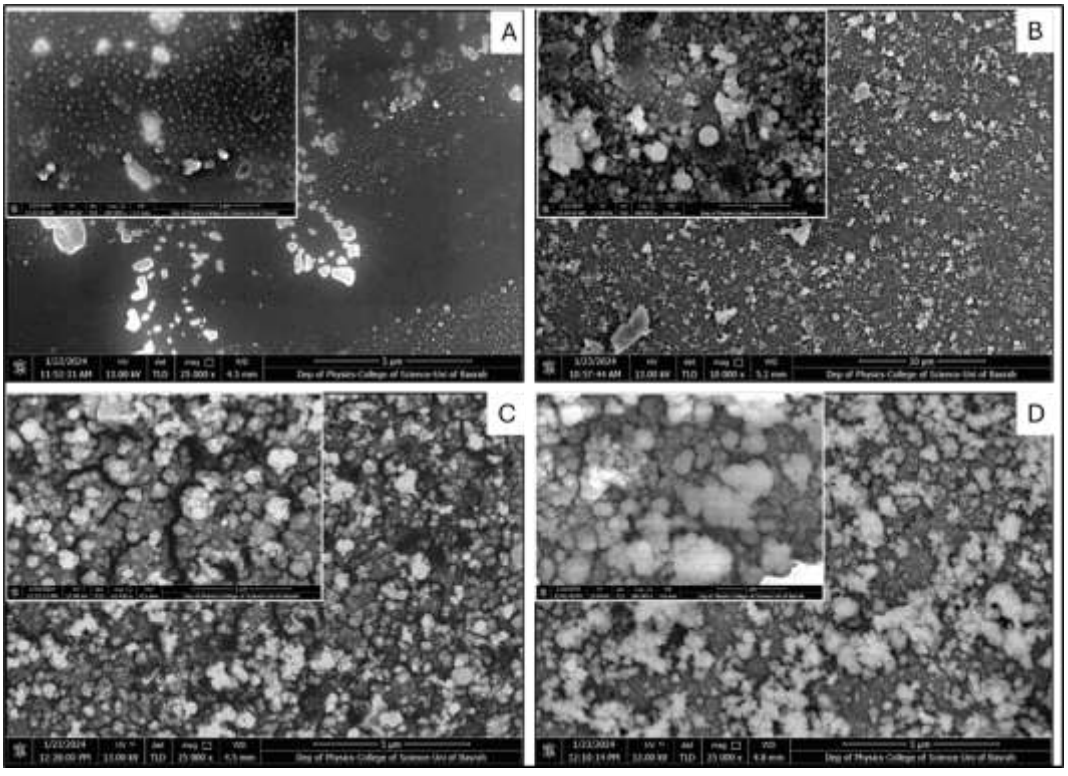

Figure 2: FESEM images show the different scale of (A) pure ZnO (B) $_{50}ZnO/_{50}SnO_2$ (C) $_{70}ZnO/_{30}SnO_2$ and (D) $_{90}ZnO/_{10}SnO_2$ for samples prepared by PLD.

The diameter range of the ZnO/SnO_2 nanocomposite thin films and pure ZnO made using the PLD method was studied. It was found that pure ZnO has an average diameter of 13 nm and a range of 5 to 50 nm. The samples of $_{50}ZnO/_{50}SnO_2$, $_{70}ZnO/_{30}SnO_2$, and $_{90}ZnO/_{10}SnO_2$ had average diameters of 15, 6.5, and 13 nm, respectively. This showed that the particles in $_{70}ZnO/_{30}SnO_2$ were the smallest, as shown in Fig. 4. The average particle size values are similar to those obtained by previous studies, ranging from 12 to 15 nm [14].

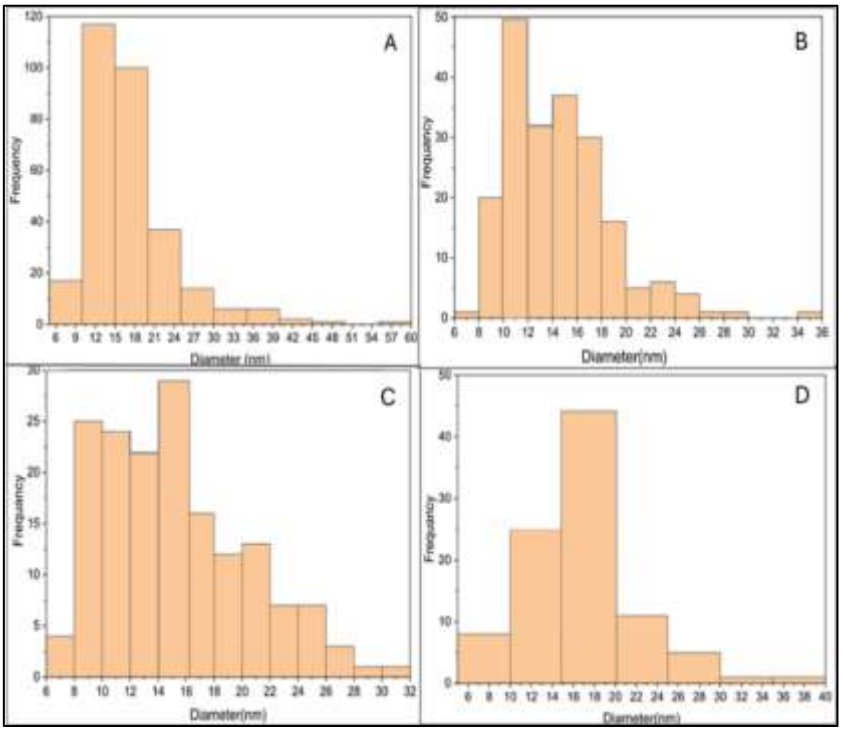

Figure 3: Diameter distribution of (A) pure ZnO (B) $_{50}ZnO/_{50}SnO_2$ (C) $_{70}ZnO/_{30}SnO_2$ and (D) $_{90}ZnO/_{10}SnO_2$ prepared by spin coating technique.

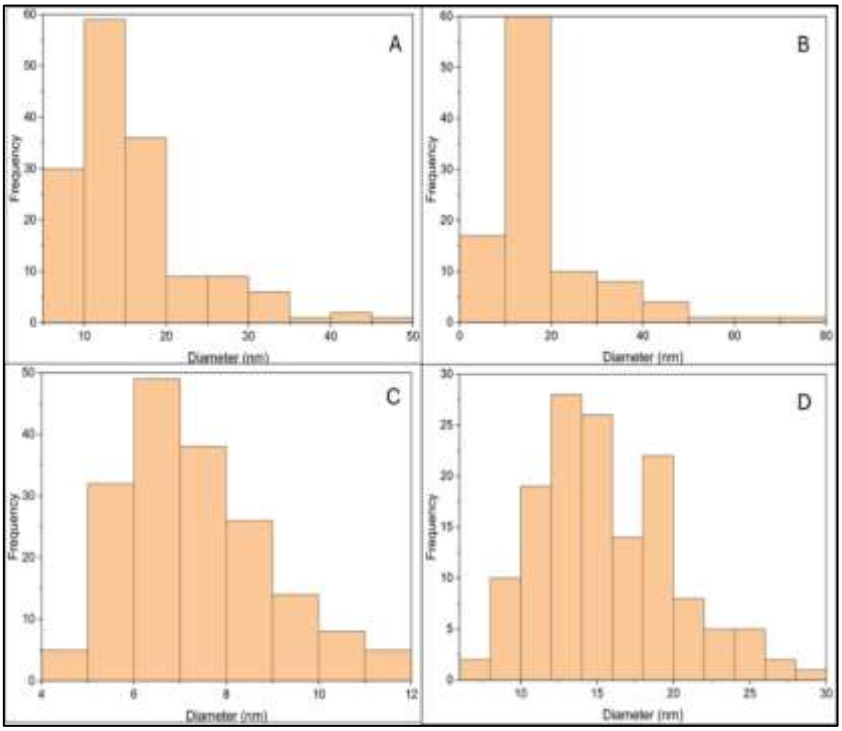

Figure 4: Diameter distribution of (A) pure ZnO (B) $_{50}ZnO/_{50}SnO_2$ (C) $_{70}ZnO/_{30}SnO_2$ and (D) $_{90}ZnO/_{10}SnO_2$ prepared by PLD technique.

3.2. X-Ray Diffraction (XRD) Analysis

The XRD patterns of pure ZnO and ZnO/SnO_2 nanocomposite thin films are shown in Figs. 5(A and B). These films were made using spin coating and PLD techniques with different concentrations of ZnO and SnO_2. The XRD patterns clearly show three prominent peaks for pure ZnO at 100, 002, and 101, which are observed at 31.6342°, 34.2892°, and 36.1233°, respectively, for the ZnO samples produced by both techniques. The nanocomposite samples of ZnO/SnO_2 exhibited, beside the prominent three peaks of ZnO, two main peaks at 26.4604° and 51.6515°, corresponding to the (110) and (211) directions of SnO_2. This demonstrates the importance of the results in fabricating the nanocomposite via spin coating and pulsed laser deposition methods, and the results agree with those of previous research [15, 16]. The synthesized nanocomposite thin films displayed the presence of two phases: the hexagonal wurtzite structure of ZnO (JCPDS No. 36-1451) [17, 18] and the tetragonal structure of SnO_2 (JCPDS No. 041-1445) [19].

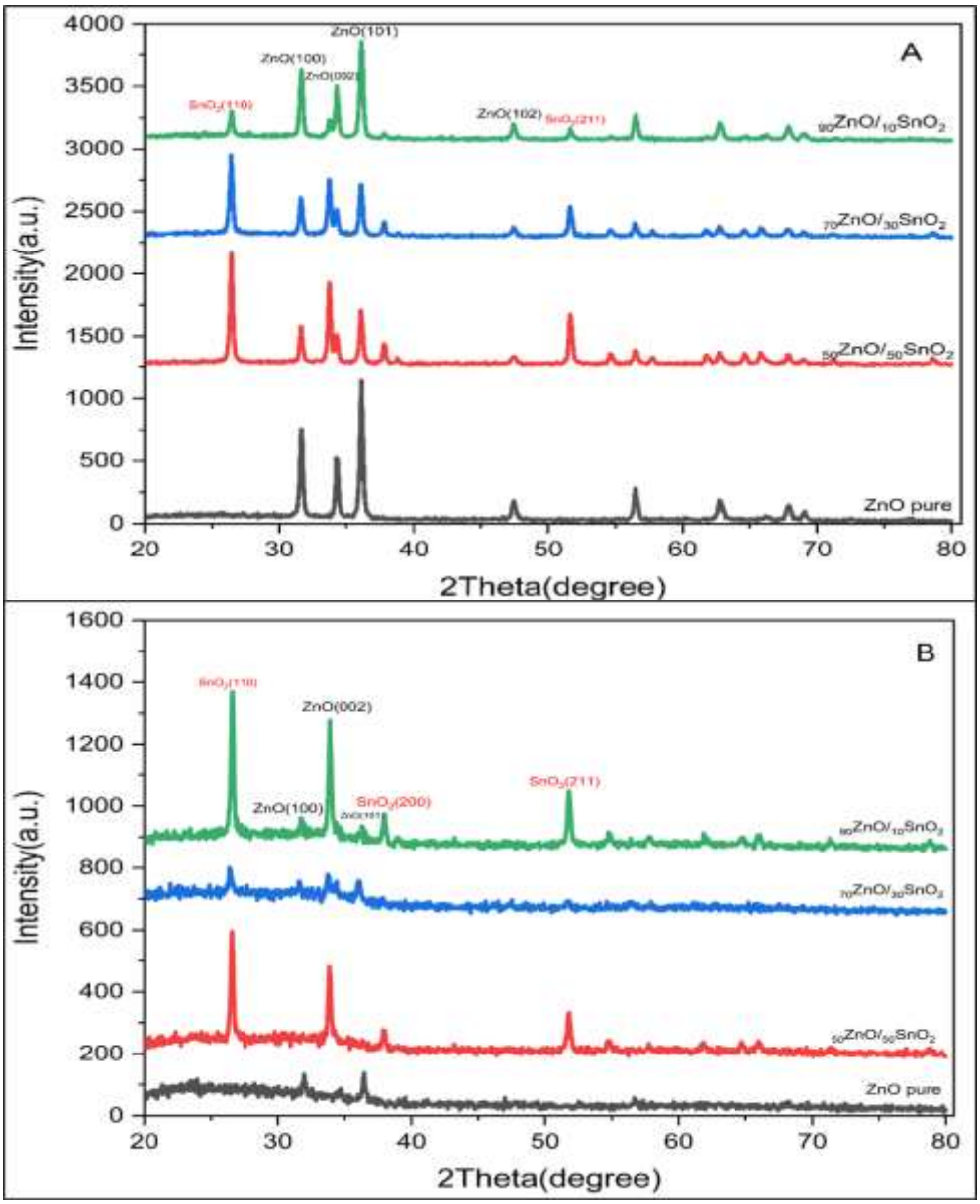

Figure 5: XRD patterns of ZnO and ZnO/SnO_2 with different concentrations (A) prepared by spin coating technique (B) prepared by PLD technique.

The crystallite grain size (D) of pure ZnO and ZnO/SnO_2 nanocomposite thin films was determined for optimal orientations utilizing Scherer's equation [20].

$$D = \frac{0.9\lambda}{\beta COS\theta} \quad (1)$$

where: λ indicates the X-ray wavelength (1.54059 Å), θ denotes the angle of diffraction, and β refers to the width of the diffraction line at half its maximum intensity in radians. The FWHM and crystallite size of pure ZnO and ZnO/SnO_2 nanocomposite thin films made by spin coating and PLD are shown in Tables 1 and 2.

Table 1: XRD parameters of ZnO/SnO_2 and pure ZnO synthesized by Spin coating technique.

SAMPLE	hkl	2Θ (degree)	FWHM (degree)	Crystallite size (nm)	Average (nm)
ZnO pure	100	31.66	0.23	35.20	35.06
	002	34.30	0.23	35.03	
	101	36.14	0.23	34.95	
$_{50}ZnO/_{50}$ SnO_2	100	31.65	0.27	30.18	31.63
	002	34.30	0.26	31.72	
	101	36.13	0.29	28.43	
	110	26.46	0.26	30.96	
	211	51.66	0.23	36.88	
$_{70}ZnO/_{30}$ SnO_2	100	31.63	0.25	36.01	34.8
	002	34.26	0.26	31.85	
	101	36.11	0.25	32.44	
	110	26.44	0.24	32.77	
	211	51.63	0.21	40.69	
$_{90}ZnO/_{10}$ SnO_2	100	31.63	0.23	35.54	35
	002	34.28	0.25	32.61	
	101	36.12	0.24	33.95	
	110	26.46	0.23	35.13	
	211	51.65	0.23	37.85	

The crystal sizes of the samples prepared via the spin coating approach varied from 35.06 nm for pure ZnO to around 35 nm for ZnO/SnO_2 nanocomposite thin films. The data in Table 1 show that the $_{50}ZnO/_{50}SnO_2$ sample had an average crystalline size of 31.63 nm. This means that the crystallite size of the samples because smaller as the SnO_2 concentration increased, which is consistent with the research results of Chaskar et al. [21].

In addition, Table 2 shows that the crystal sizes of the samples prepared using the PLD method ranged from 27 nm for ZnO to about 37.76 nm for the nanocomposite samples. The $_{70}ZnO/_{30}SnO_2$ nanocomposite had the smallest average crystal size of 15.27 nm**.** This variation in results is due to the preparation conditions as well as the increase in structural defects [15].

3. 3. Optical Analyses

Fig. 6 illustrates the optical absorption spectra of pure ZnO and ZnO/SnO_2 nanocomposite thin films produced using spin coating and pulsed laser deposition at different concentrations. The absorption decreases for longer wavelengths or lower photon energies, as seen in Fig. 6. The material exhibited significant reflective properties and a rapid decrease in absorption beyond 400 nm. The samples produced via the pulsed laser deposition method exhibited greater absorbance than those produced by

spin coating, particularly the $_{70}ZnO/_{30}SnO_2$ nanocomposite thin film. In all methods, adding SnO_2 enhanced the absorbance compared to pure ZnO. The enhancement could arise from the improved crystalline quality of the ZnO/SnO_2 nanocomposite thin films, as indicated by the XRD results.

Table 2: XRD parameters of ZnO/SnO_2 and pure ZnO synthesized by PLD technique.

Sample	hkl	2Θ (degree)	FWHM (degree)	Crystallite size (nm)	Average (nm)
ZnO pure	100	31.98	0.34	24.02	27.68
	002	34.69	0.26	31.21	
	101	36.47	0.30	27.81	
$_{50}ZnO/_{50}\ SnO_2$	100	31.22	0.34	24.02	29.48
	002	34.31	0.26	31.21	
	101	36.35	0.30	27.81	
	110	26.58	0.25	32.49	
	200	37.94	0.26	31.90	
$_{70}ZnO/_{30}\ SnO_2$	100	31.58	0.69	11.90	15.27
	002	34.31	0.56	14.84	
	101	36.08	0.52	15.90	
	110	26.46	0.55	14.67	
	200	37.85	0.44	19.0	
$_{90}ZnO/_{10}\ SnO_2$	100	31.66	0.30	27.40	37.76
	002	34.39	0.16	49.50	
	101	36.26	0.24	34.19	
	110	26.61	0.22	36.66	
	211	51.78	0.21	41.52	

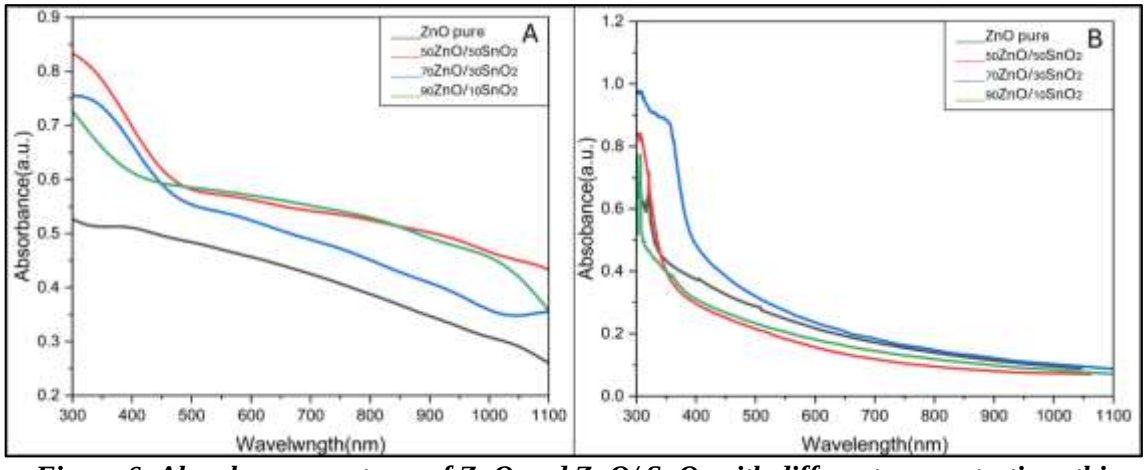

Figure 6: Absorbance spectrum of ZnO and ZnO/ SnO_2 with different concentrations thin films: A) prepared by spin coating B) prepared by PLD method.

Figs. 7 and 8 illustrate the Tauc plot for pure ZnO, $_{50}ZnO/_{50}SnO_2$, $_{70}ZnO/_{30}SnO_2$, and $_{90}ZnO/_{10}SnO_2$ nanocomposite thin films. The optical band gap, E_g, of the synthesized samples was determined by applying the linear portion of α^2 versus hv plots utilizing the following equation [22].

$$(\alpha h\nu)^2 = A(h\nu - E_g)^n \quad \textbf{(2)}$$

where: α indicates the absorption coefficient, hv refers to the photon energy, Eg is the optical band-gap energy, and A is a constant that depends on the electron-hole mobility.

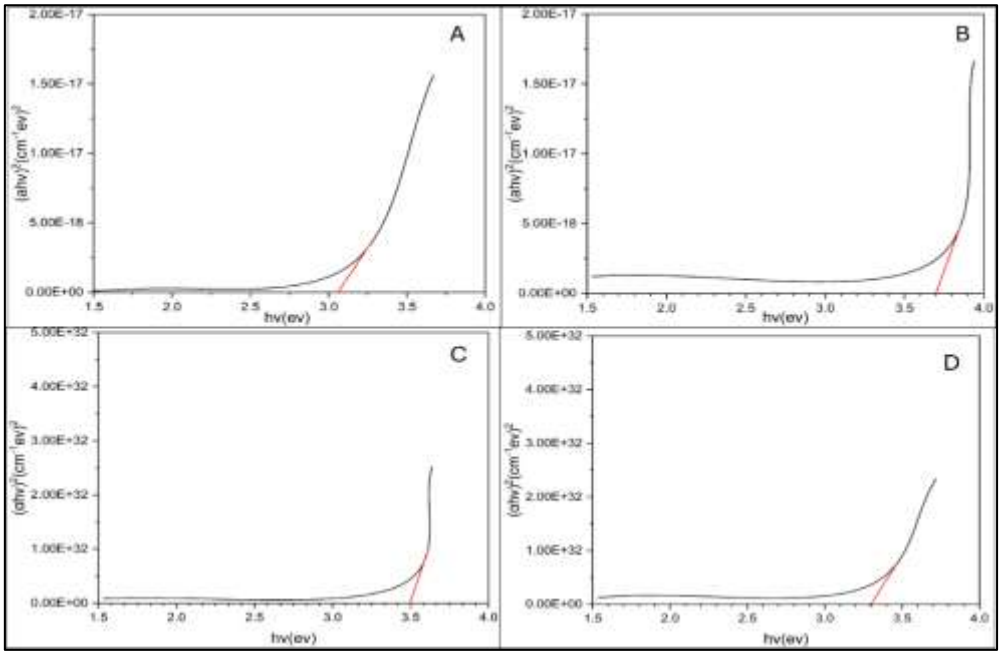

Figure 7: Tauc plots of ZnO and ZnO/SnO2 thin films with different concentrations (A) pure ZnO (B) $_{50}$ZnO/$_{50}$SnO$_2$ (C) $_{70}$ZnO/$_{30}$SnO$_2$ and (D) $_{90}$ZnO/$_{10}$SnO$_2$ prepared by spin coating technique.

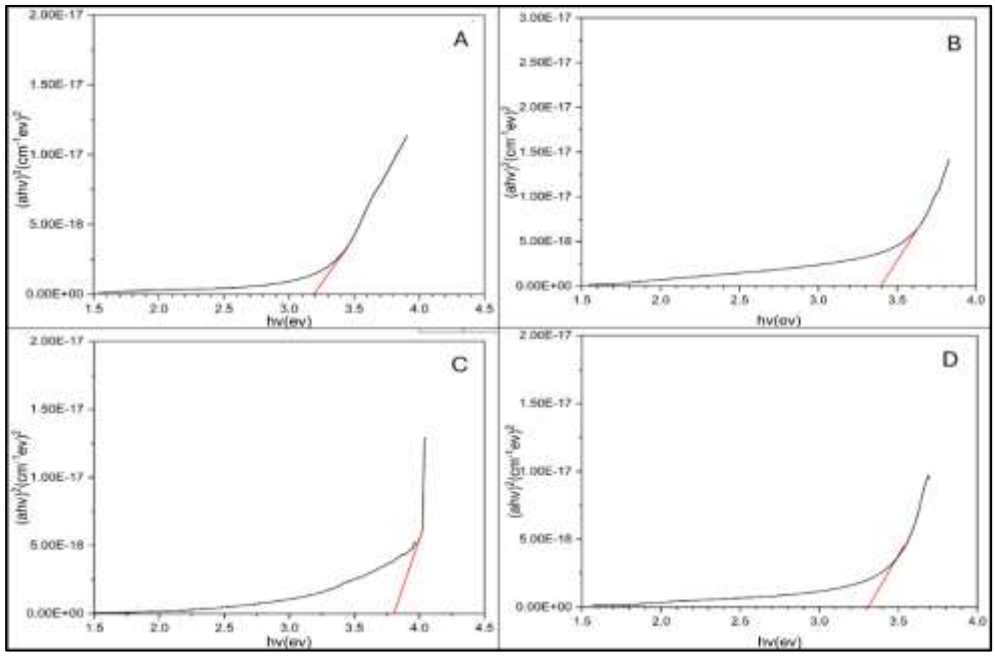

Figure 8: Tauc plots of ZnO and ZnO/SnO$_2$ thin films with different concentrations (A) pure ZnO (B) $_{50}$ZnO/$_{50}$SnO$_2$ (C) $_{70}$ZnO/$_{30}$SnO$_2$ and (D) $_{90}$ZnO/$_{10}$SnO$_2$ prepared by PLD method technique

.

The band gap energy of samples produced via spin coating varied from 3.2 eV for pure ZnO to around 3.8 eV for the $_{50}$ZnO/$_{50}$SnO$_2$ nanocomposite samples, indicating that the band gap increased with the concentration of SnO$_2$ [23]. On the other hand, Table 3 indicates that the energy gap of nanocomposite thin films synthesized via the

PLD method increased to 3.7 eV. This is due to the direct energy gap excitations of ZnO and SnO_2, which are around 3.3 eV and 3.6 eV, respectively [24, 25].

Table 3: The optical energy gaps of ZnO and ZnO/SnO_2 thin films with different composite prepared by spin coating and PLD method.

Sample	E_g (eV) spin coating	E_g (eV) PLD
ZnO pure	3.2	3.2
$_{50}ZnO/_{50}SnO_2$	3.8	3.4
$_{70}ZnO/_{30}SnO_2$	3.5	3.7
$_{90}ZnO/_{10}SnO_2$	3.3	3.3

The addition of SnO_2 resulted in subtle blue shifts of the absorption edge, indicating that the mixture of ZnO and SnO_2 enhances the band gap energy of the nanocomposite samples. The interface between these two materials in the composite may introduce energy barriers that influence the electronic characteristics, leading to an increase in the band gap [21, 23].

4. Conclusions

The physical properties of pure ZnO and ZnO/SnO_2 nanocomposites, prepared using spin coating and PLD, were analyzed, including their morphological, structural, and optical attributes. Pure ZnO has a diameter range of 4 to 45 nm. The pure ZnO and ZnO/SnO_2 nanocomposite thin films, produced using the spin coating method, exhibited an average particle size increase from 11 to 18 nm when the ZnO ratio increased from 50% to 90%. The smallest particle size for samples produced using PLD was 6.5 nm, obtained with a ZnO:SnO_2 ratio of 70:30. The XRD patterns show three clear peaks for pure ZnO at indices 100, 002, and 101, which correspond to angles of 31.6342°, 34.2892°, and 36.1233°, respectively. These peaks can be seen using both methods. In addition to the obvious three peaks of ZnO, the nanocomposite samples of ZnO/SnO_2 displayed two main peaks at 26.4604° and 51.6515°, which corresponded to the (110) and (211) orientations of SnO_2. Both methods produced pure ZnO with optical energy gaps of 3.2 eV. The energy gap of the $_{50}ZnO/_{50}SnO_2$ nanocomposite, manufactured using spin coating, was demonstrated to increase to 3.8 eV. The PLD method demonstrated the energy gap of the $_{70}ZnO/_{30}SnO_2$ nanocomposite at 3.7 eV.

Conflict of Interest

The authors declare that they have no conflict of interest.

References

1. Z. Huang, J. Zhu, Y. Hu, Y. Zhu, G. Zhu, L. Hu, Y. Zi, and W. Huang, Nanomaterials **12**, 632 (2022). DOI: 10.3390/nano12040632.
2. N. H. Al-Mutairi, A. H. Mehdi, and B. J. Kadhim, European J. Res. Develop. Sust. **3**, 102 (2022).
3. V. V. Petrov, V. V. Sysoev, A. P. Starnikova, M. G. Volkova, Z. K. Kalazhokov, V. Y. Storozhenko, S. A. Khubezhov, and E. M. Bayan, Chemosensors **9**, 124 (2021). DOI: 10.3390/chemosensors9060124.
4. J. Song, E. Zheng, X.-F. Wang, W. Tian, and T. Miyasaka, Sol. Ener. Mat. Sol. Cell. **144**, 623 (2016). DOI: 10.1016/j.solmat.2015.09.054.
5. Y. Yang, S. Li, F. Liu, N. Zhang, K. Liu, S. Wang, and G. Fang, J. Lumin. **186**, 223 (2017). DOI: 10.1016/j.jlumin.2017.02.043.
6. X. Wang, X. Wang, Q. Di, H. Zhao, B. Liang, and J. Yang, Materials **10**, 1398 (2017). DOI: 10.3390/ma10121398.
7. A. Guerram, S. E. Laouini, H. A. Mohammed, G. G. Hasan, M. L. Tedjani, F. Alharthi, and F. Menaa, J. Clus. Sci. **35**, 2231 (2024). DOI: 10.1007/s10876-024-02642-9.

8. B. Mondal, B. Basumatari, J. Das, C. Roychaudhury, H. Saha, and N. Mukherjee, Sens. Actuat. B Chem. **194**, 389 (2014). DOI: 10.1016/j.snb.2013.12.093.
9. A. A. Hussain and Q. N. Abdullah, Tikrit J. Pure Sci. **28**, 66 (2023). DOI: 10.25130/tjps.v28i6.1379.
10. A. Saldaña-Ramírez, M. R. A. Cruz, I. Juárez-Ramírez, and L. M. Torres-Martínez, Opt. Mat. **110**, 110501 (2020). DOI: 10.1016/j.optmat.2020.110501.
11. S. K. Sinha, T. Rakshit, S. K. Ray, and I. Manna, Appl. Surf. Sci. **257**, 10551 (2011). DOI: 10.1016/j.apsusc.2011.07.049.
12. N. D. Md Sin, A. K. Shafura, M. F. Malek, M. H. Mamat, and M. Rusop, IOP Conf. Ser. Mater. Sci. Eng. **83**, 012002 (2015). DOI: 10.1088/1757-899X/83/1/012002.
13. S. W. Lee, Y.-W. Kim, and H. Chen, Appl. Phys. Lett. **78**, 350 (2001). DOI: 10.1063/1.1337640.
14. E. M. Bayan, V. V. Petrov, M. G. Volkova, V. Y. Storozhenko, and A. V. Chernyshev, J. Adv. Dielect. **11**, 2160008 (2021). DOI: 10.1142/S2010135X21600080.
15. H. F. Al Taay, Y. T. Mohammed, and H. F. Oleiwi, Iraqi J. Phys. **18**, 40 (2020). DOI: 10.30723/ijp.v18i45.536.
16. H. D. Abdullah, H. F. Al-Taay, M. K. Khalaf, H. F. Oleiwi, and A. J. Rahma, J. Phys.: Conf. Ser. **2114**, 012074 (2021). DOI: 10.1088/1742-6596/2114/1/012074.
17. S. Karakaya, J. Mat. Sci. Mat. Elect. **29**, 4080 (2018). DOI: 10.1007/s10854-017-8352-x.
18. M. A. Benali, H. Tabet Derraz, I. Ameri, A. Bourguig, A. Neffah, R. Miloua, I. E. Yahiaoui, M. Ameri, and Y. Al-Douri, Mat. Chem. Phys. **240**, 122254 (2020). DOI: 10.1016/j.matchemphys.2019.122254.
19. A. H. Yahi, A. Bouzidi, R. Miloua, M. Medles, A. Nakrela, M. Khadraoui, H. Tabet-Derraz, R. Desfeux, A. Ferri, and J. F. Blach, Optik **196**, 163198 (2019). DOI: 10.1016/j.ijleo.2019.163198.
20. Z. J. Shanan, S. M. Hadi, and S. K. Shanshool, Baghdad Sci. J. **15**, 0211 (2018). DOI: 10.21123/bsj.2018.15.2.0211.
21. M. Chaskar, V. Kadam, C. Jagtap, N. Naik, S. S, E. Jadkar, H. Pathan, and P. Adhyapak, ES Ener. Envir. **26**, 1250 (2024). DOI: 10.30919/esee1250.
22. N. Talebian, M. R. Nilforoushan, and E. B. Zargar, Appl. Surf. Sci. **258**, 547 (2011). DOI: 10.1016/j.apsusc.2011.08.070.
23. N. a. Y. Abduh and A.-B. Al-Odayni, Materials **16**, 7398 (2023). DOI: 10.3390/ma16237398.
24. A. Kahraman, E. Socie, M. Nazari, D. Kazazis, M. Buldu-Akturk, V. Kabanova, E. Biasin, G. Smolentsev, D. Grolimund, E. Erdem, J. E. Moser, A. Cannizzo, C. Bacellar, and C. Milne, J. Phys. Chem. Lett. **15**, 1755 (2024). DOI: 10.1021/acs.jpclett.3c03519.
25. M. Karmaoui, A. B. Jorge, P. F. Mcmillan, A. E. Aliev, R. C. Pullar, J. A. Labrincha, and D. M. Tobaldi, ACS Omega **3**, 13227 (2018). DOI: 10.1021/acsomega.8b02122.

تصنيع ودراسة الخصائص التركيبية والبصرية لأغشية المركبات النانوية الرقيقة المحضرة بطريقة الطلاء الدوراني والترسيب بالليزر النبضي

امنه احمد رشيد[1] وهناء فليح الطائي[1]

[1]قسم الفيزياء، كلية العلوم للبنات، جامعة بغداد، بغداد، العراق

الخلاصة

يتم تحضير أفلام رقيقة من مركب ZnO/SnO_2 النانوي على ركائز زجاجية باستخدام تقنيات الطلاء الدوراني والترسيب بالليزر النبضي (PLD)، مع استخدام نسب مختلفة من ZnO/SnO_2 تتعرض الأفلام الرقيقة المصنعة للتسخين عند 300 درجة مئوية لتحسين بلورتها .يتم فحص مورفولوجيا السطح، الهيكل البلوري، والخصائص البصرية للأفلام الرقيقة الناتجة من نانوكومبوزيت ZnO/SnO_2 .أظهرت صور FESEM لأفلام ZnO و ZnO/SnO_2 النانوية المركبة التي تم تصنيعها عبر عملية الطلاء الدوراني زيادة في حجم الجسيمات من 11 إلى 18 نانومتر عندما زادت نسبة ZnO من 50% إلى 90% .أقل حجم للجسيمات في العينات التي تم إنتاجها باستخدام تقنية PLD كان 6.5 نانومتر، وتم تحقيقه بنسبة $ZnO:SnO_2$ تبلغ 70:30 .أشارت نتائج حيود الأشعة السينية (XRD) إلى أن الأفلام الرقيقة من ZnO وZnO/SnO_2النانوية المركبة، التي تم تحضيرها باستخدام طرق الطلاء الدوراني وPLD، أظهرت الهيكل السداسي الزاوية لويرتزايت ZnO والهيكل الرباعي الزاوية لـSnO_2 فجوة الطاقة البصرية لـ ZnO النقي الناتج عن كلا الطريقتين كانت 3.2 إلكترون فولت، والتي زادت إلى 3.8 إلكترون فولت لأفلام رقيقة من نانوكومبوزيت $50ZnO/50SnO_2$ المحضرة باستخدام طريقة الطلاء الدوراني .كان فجوة الطاقة لأفلام النانو المركبة $70ZnO/30SnO_2$ تساوي 3.7 إلكترون فولت عند استخدام طريقة والترسيب بالليزر النبضي.

الكلمات المفتاحية: ZnO،SnO_2 ، مركبات نانوية، ترسيب بالليزر النبضي، الطلاء الدوراني.